Extended Fabrication-Aware Convolution Learning Framework for Predicting 3D Shape Deformation in Additive Manufacturing

Yuanxiang Wang¹, Cesar Ruiz¹ and Qiang Huang¹

Abstract—Geometric accuracy control is critical for precision additive manufacturing (AM). To learn and predict the shape deformation from a limited number of training products, a fabrication-aware convolution learning framework has been developed in our previous work to describe the layer-by-layer fabrication process. This work extends the convolution learning framework to broader categories of 3D geometries by constructively incorporating spherical and polyhedral shapes into a unified model. It is achieved by extending 2D cookie-cutter modeling approach to 3D case and by modeling spatial correlations. Methodologies demonstrated with real case studies show the promise of prescriptive modeling and control of complicated shape quality in AM.

I. Introduction

As a revolutionary technology, additive manufacturing (AM) or three-dimensional (3D) printing enables the direct fabrication of products with highly complex geometries through layer-by-layer fabrication using various materials including metals, ceramics, polymers, and their composites, hybrid, or functionally graded materials. Unlike traditional manufacturing methods, AM has the potential of building extremely complex geometries with high efficiency and low material waste. However, one major barrier for broader adoption of AM techniques is the geometric shape inaccuracy. Due to a wide spectrum of AM processes, low sample size caused by one-of-a-kind manufacturing and complicate geometries, accuracy control has been a daunting task for researchers and practitioners [1], [2], [3], [4], [5], [6], [7], [8], [9], [10].

Three types of methodologies have been reported to improve the shape accuracy: (1) physics-based modeling and simulation based on first-principles; (2) data-driven modeling using statistical and machine learning (ML) techniques; and (3) physics-informed ML modeling by incorporating process knowledge into modeling and learning. One major part of physics-based modeling strategies applies finite element methods (FEM) to predict the final product quality [11], [12]. For example, King et al. [13] proposed a multi-scale modeling approach based on the comprehensive physical understanding of both the powder scale and the part scale to predict shape accuracy, residual stress, and material properties of the laser powder bed fusion process. Similarly, Yan et al. [14] proposed a micro-scale model for electron-material

¹Yuanxiang Wang, Cesar Ruiz, and Qiang Huang are with the Daniel J. Epstein Department of Industrial and Systems Engineering, University of Southern California, Los Angeles, CA 90007, USA, yuanxian@usc.edu, cesarrui@usc.edu, qiang.huang@usc.edu

interaction, a meso-scale model for powder particle evolution, and a macro-scale model using FEM. These models can achieve voxel-level accuracy for describing 3D products along the printing process, but at a high computational cost. Moreover, the development of such models requires extensive expert's knowledge and the models are restricted to a specific type of AM processes and/or materials.

To improve the printing accuracy, process optimization have long been employed with both online and offline observations [15]. For instance, Anderegg et al. [16] monitored in-situ temperature and pressure inside the nozzle of a fused filament fabrication printer to minimize their fluctuation during fabrication process. To reduce the slicing error incurred when transforming the computer-aided design (CAD) to the building file, Mao et al. [17] optimized the slicing plan and building orientation by considering multiple metric profiles including cusp height, surface roughness, area deviation, and volume deviation.

For building data-driven models, machine learning strategies has been explored by using in-situ monitoring data such as thermal history and optical sensing data. Francis and Bian [18] applied deep learning to predict the top surface distortion of disks through a combination of convolution neural network (CNN) and artificial neural network using thermal history data collected during the printing process. To enable learning from different shapes, Decker et al. [19] employed a random forest method to predict the shape deformation of an untried shape by extracting position, geometry and material expansion features from the triangular meshes of other shapes in the FDM process. Many efforts have been taken to enable model transfer across materials, fabrication processes and shapes to improve prediction accuracy with a limited number of printed parts. For example, Chen et al. [20] achieved the knowledge transfer across different shapes by decomposing the geometric error into shapeindependent and shape-specific components, and then fixing the global shape-independent parameters and shape features, respectively. Ferreira et al. [21] proposed a Bayesian extreme learning machine methodology to automatically predict the shape deformation pattern of freeform shapes under different printing processes by using knowledge of the shape deformation patterns of simpler shapes printed under the same and different processes. These transfer learning methods are limited to 2D shapes.

The physics-informed ML aims to predict the shape deformation of arbitrary shapes using a limited number of training products and construct compensation plans to improve the quality of new parts [22]. This strategy has

been successfully implemented for thin (in height) shapes that can be approximated as 2D shapes for purposes of shape deviation modeling. Huang et al. [3] developed a prescriptive statistical modeling approach to predict and compensate the 2D shape deformation of circular shapes considering the size effect and over-exposure, which serves as a basis for a series of following work. A key challenge to model polygonal shapes is that the deformation pattern changes dramatically on the sharp corners. To transfer the knowledge from circular shape deformations to that of regular polygons, Huang et al. [4] proposed the use of a cookie-cutter function that is parameterized by the number of sides, which cuts the polygons from their circumcircles. After modeling the shape deformation of circular and polygonal shapes, Luan and Huang [5] predicted the shape deformation of 2D freeform products considering a piecewise approximation with circular or polygonal sections and applied the compensation plan that modifies CAD design to control geometric inaccuracy.

The modeling and control issues faced in printing 2D shapes are exacerbated for 3D cases, since the deformation pattern can change from layer-to-layer due to complex process physics including inter-layer interactions [23], [24], [25], [26]. To incorporate the layer-by-layer fabrication mechanism into modeling and learning, Huang et al. [9] proposed a convolution learning framework to describe the 3D deformation patterns as the result of the 2D shape deformation of each layer convolved with a transfer function that captures inter-layer interactions. Although this framework was validated with spherical shapes built in a stereolithography (SLA) process, it still requires fundamental work to predict the complex deformation patterns of freeform shapes. In particular, a purely convolution formulation over-smooths the deformation profiles observed on the sharp corners of 3D printed products. In this paper, a consistent modeling framework for spherical and polyhedral shapes is proposed. The main reason to study these particular shapes is that 3D freeform shapes can be approximated as a combination of spherical and polyhedral patches. Understanding of these two basic categories of 3D shapes makes it possible for 3D freeform shape prediction, just as the work demonstrated for 2D case [3], [4], [5]

The remainder of this paper is organized as follows. Sec. II briefly reviews the convolution framework proposed in [9] and proposes a unified model for a broader category of shapes by introducing a new set of functions that capture the effect of polyhedral geometries on the deviation profile. In Sec. III, joint modeling of shape deformation for domes and thin walls with half-cylindrical shapes is investigated. Conclusion and future work are given in Sec. IV.

II. A Unified Convolution Learning Framework for Deformation Modeling

This section briefly introduces the convolution learning framework for modeling shape deformation of AM built products. A new 3D cookie-cutter function is proposed to extend the learning framework in order to capture the complex shape deformation profiles for polyhedral shapes.

Furthermore, a Gaussian process with a Euclidean distance metric is introduced to characterize the spatial correlation among neighboring regions.

A. Deformation Modeling of Spherical Products Through Convolution Framework

In [9], the convolution learning framework was proposed as

$$y(\mathbf{x}) = (f * g)(\mathbf{x}) + \mathcal{GP}(0, k(\cdot, \cdot)) + \epsilon, \tag{1}$$

where $y(\mathbf{x})$ is the shape deviation, \mathbf{x} are the features, f is the input function that models the 2D shape deformation in a horizontal layer, g is the transfer function that models the layer-to-layer interactions, $\mathcal{GP}\left(0,k\left(\cdot,\cdot\right)\right)$ is a mean-zero Gaussian process with covariance kernel function k that captures the spatial correlation, and ϵ is the measurement error that follows a normal distribution with mean 0 and variance σ^2 .

The deformation $y(\mathbf{x})$ of a 3D printed product from its designed shape is described using the spherical coordinate system (SCS) with dimensions (r,θ,φ) , where θ is the polar angle and φ is the azimuth angle. The measurement point cloud is represented as $r(\theta,\varphi)$ and the designed shape is denoted as $r_0(\theta,\varphi)$. Thus, shape deformation is defined as $y(\mathbf{x}) = r(\theta,\varphi) - r_0(\theta,\varphi)$, where $\mathbf{x} = (r_0(\theta,\varphi),\theta,\varphi)$, $\theta \in [0,2\pi)$, and $\varphi \in [0,\pi/2]$.

The first step of the convolution learning framework is to identify the input function f, which describes the in-plane shape deformation. For 3D spherical shapes (domes), each layer is a circle. Shape deformation for circles of radius r_0 can often be modeled with a few Fourier basis functions [3], for example, $f(r_0,\theta)=c_1(r_0)+c_2(r_0)\cos(2\theta)$. Using this function, Huang et al. [9] modeled the deformation of a dome shape as

$$y(r_0, \theta, \varphi) = \beta(r_0) + \alpha(r_0)(f * g)(\theta, \varphi) + \mathcal{GP}(0, k(\cdot, \cdot)) + \epsilon.$$
(2)

Then, the size factors $c_1(r_0)$ and $c_2(r_0)$ can be absorbed in $\alpha(r_0)$ and $\beta(r_0)$ in Eq. (2). Since each layer of a dome shape has radius $r_0 \sin \varphi$, the input function for the domes can be normalized, for example, as

$$f(\theta, \varphi) = \cos(2\theta)\sin\varphi. \tag{3}$$

For the transfer function $g(\mathbf{x})$, LASSO [27] model selection was adopted as

$$\min_{\mathbf{c}} \quad \frac{1}{N} \sum_{i=1}^{N} \left(y_i - \sum_{j} c_j (f * g_j)(\theta_i, \varphi_i) \right)^2 + \gamma ||\mathbf{c}||_1, \tag{4}$$

where N is the number of sampled points and $g_j(\theta,\varphi)$ is a 2-D Fourier basis function. Significant terms shared among all domes were selected and the final form of the transfer function was

$$g(\theta, \varphi) = \cos(n_1 \varphi) [1 + \cos(n_2 \theta + \psi)]. \tag{5}$$

Lastly, Gaussian process regression (GPR) over the parametric model residuals $\bar{y}\left(r_0,\theta,\varphi\right)=y\left(r_0,\theta,\varphi\right)-\hat{\beta}(r_0)$

 $\hat{\alpha}(r_0)(f*g)(\theta,\varphi)$ was conducted to take account for the remaining high-order spatial correlation of the deviation profile.

B. Extended Convolution Learning Framework for Shape Deformation

Although the convolution framework shown in Eq. (2) is quite general, it struggles to learn the sharp transitions observed in the deviation profiles around the corners of polyhedral shapes (shown in Fig. 3) because the convolution combines the smoothness of both f and g functions. Moreover, using an excessive number of basis functions would lead to over-fitting.

In the 2D case, a cookie-cutter function $f_2(\theta, r_0(\theta))$ was proposed in [4] to link the deformation of circular shapes to that of polygons as

$$f(\theta, r_0(\theta)) = f_1(\theta, r_0(\theta)) + f_2(\theta, r_0(\theta)) + f_3(\theta, r_0(\theta)) + \epsilon,$$
(6)

where $f_1(\theta, r_0(\theta))$ describes circular shape deformation and $f_3(\theta, r_0(\theta))$ is a high-order term.

To generalize this idea to 3D cases, we model each layer of a polyhedral shape as a polygon being cut from its circumcircle, then the whole product can be carved out from the stack of circular shapes. Thus, we can extend the convolution learning framework to spherical and polyhedral shapes as an additive model of the base function for spherical shapes, a 3D cookie-cutter function, and a high-order term for the remaining pattern.

By denoting the convolution term in Eq. (2) as

$$h_1(\theta, \varphi) = (f * q)(\theta, \varphi), \tag{7}$$

the extended convolution learning model can be written as

$$y(r_0(\theta, \varphi), \theta, \varphi) = \alpha_0(r_0) + \alpha_1(r_0)h_1(\theta, \varphi)$$

$$+ \alpha_2(r_0)h_2(\theta, \varphi)$$

$$+ \alpha_3(r_0)h_3(\theta, \varphi)$$

$$+ \mathcal{GP}(0, k(\cdot, \cdot)) + \epsilon,$$

$$(8)$$

where the first row corresponds to the model in Eq. (2) describing spherical shape deformation, h_2 is the 3D cookie-cutter function, and h_3 represents the remaining high-order pattern. Note that h_1 can be learned from spherical products as in [9], and both h_2 and h_3 are fully determined by the geometries of AM fabricated products.

For 3D geometries, we extend the 2D cookie-cutter function square.wave(θ) = sign{ $\cos[n(\theta-\phi_0)/2]$ } proposed in [4] and modify the frequency as

$$h_2(\theta, \varphi) = \frac{1}{2} \left\{ \text{sign} \left[\sin \left(\frac{(-1)^{j+1} \pi \theta}{\vartheta_j(\varphi)} \right) \right] + 1 \right\}, \quad (9)$$

for $\vartheta_{j-1}(\varphi) \leq \theta < \vartheta_j(\varphi), \quad j=1,\dots,n+1$, where $\vartheta_j, j=1,\dots,n$ are the polar angles of sharp transitions with $\vartheta_0(\varphi)=0$ and $\vartheta_{n+1}(\varphi)=2\pi$. It can be regarded as the stack of 2D cookie-cutter functions over the φ -direction, where each layer could have sharp transitions at different angles according to the designed geometry.



Fig. 1. Thin walls with half-cylindrical shapes printed in an SLA process

As an example, considering the thin wall with a half-cylindrical shape that has radius r_0 and thickness D as shown in Fig. 1, each horizontal layer is a rectangle with length $2r_0\sin\varphi$ and width D. To cut out a rectangular $A_1A_2A_3A_4$ from its circumscircle as shown in Fig. 2(a), we first find the angles of each corner as $\vartheta_1, \vartheta_2, \vartheta_3$ and ϑ_4 , which incurs the 2-D cookie-cutter function shown in Fig. 2(b). Since the rectangle sides in each horizontal layer defined by φ are different, the sharp transitions for each layer happen at different polar angles, which are purely defined by the geometry of the product.

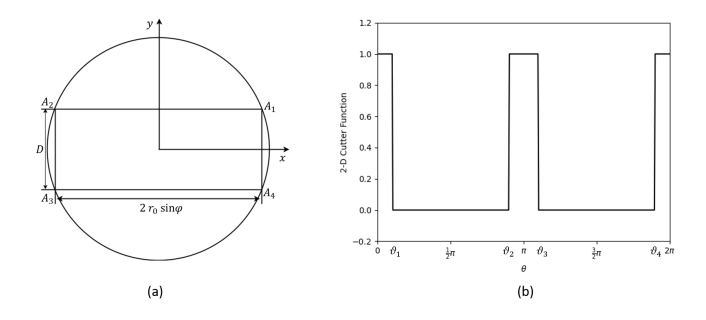


Fig. 2. A rectangle cut from its circumcircle and corresponding 2D cookiecutter function

III. CASE STUDY FOR METHODOLOGY VALIDATION

In this section, we demonstrate the capability of the extended convolution learning framework in Eq. (8) for learning and predicting the shape deviation patterns of a wide variety of geometries containing both spherical and polyhedral shapes. The small training data contains domes and thin walls with half-cylindrical shapes.

A. AM Experiments and Observations

The AM process for this work is the mask image projection stereolithography (MIP-SLA) developed by Envision-TEC. Unlike the traditional SLA process, MIP-SLA projects the sliced mask images dynamically onto a resin surface to build the product. After the printing process, ROMER absolute arm with RS4 laser scanner is used to collect the measurements as point clouds, which are then registered using the well-known iterative closest point algorithm [28].

For spherical products, we use domes with radii 0.5 inch, 0.8 inch, 1.5 inches and 1.8 inches that studied in [9] as the training set. Three 0.25-inch-thick thin walls with half-cylindrical shapes that have radii of 0.8 inch, 1.5 inches, and 2.0 inches, respectively, were vertically printed at the center of the printing platform as shown in Fig. 1. We employ

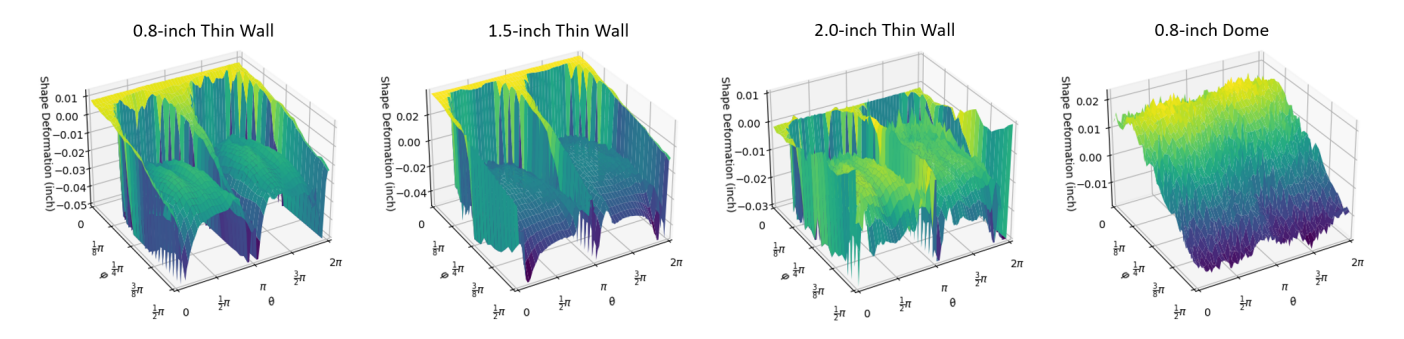


Fig. 3. Shape deformation measurements of three thin walls with half-cylindrical shapes and the 0.8-inch dome presented in SCS

the 0.8-inch and 2.0-inch thin walls as the training set and leave the 1.5-inch thin wall as the validation set. Their shapedeviation profiles on the SCS are presented in Fig. 3. We also include the shape deformation of the 0.8-inch dome from [9] for comparison. It is obvious that the deformation pattern of the thin walls differs significantly from the dome shape.

B. Convolution Modeling and Learning

To adopt the convolution learning framework in Eq. (8), the first step is to identify the input function f. Note that, due to machine repair, the pattern of shape deformation of 2D circular disks changed from what was presented in [3], i.e., the input function $f(\theta, \varphi)$ should have a different pattern and we need to fit the spherical shape model for the new data. We can extract the pattern from the fitted model for circular shape deformation from Luan and Huang [5] as

$$f(\theta) = \cos\left(2\theta + \frac{\pi}{3}\right) \mathbf{1}_{\theta \in [0,\pi)} - \sin(2\theta) \mathbf{1}_{\theta \in [\pi,2\pi)}. \quad (10)$$

Recall that the form of input function was changed to Eq. (3) by multiplying it by $\sin \varphi$ because the radius of each layer is $r_0 \sin \varphi$ for the dome shape. Similarly, we have the input function $f(\theta, \varphi)$ for spherical shapes as

$$f(\theta, \varphi) = \left[\cos\left(2\theta + \frac{\pi}{3}\right)\mathbf{1}_{\theta \in [0, \pi)} - \sin(2\theta)\mathbf{1}_{\theta \in [\pi, 2\pi)}\right] \sin\varphi.$$
(11)

If the radius is r_0 and the thickness is D for the thin wall shape, the circumcircle radius for each horizontal layer φ is

$$\max_{\theta} \{ r_0(\theta, \varphi) \} = \sqrt{r_0^2 \sin^2 \varphi + \left(\frac{D}{2}\right)^2} \approx r_0 \sin \varphi, \quad (12)$$

since D is much smaller than r_0 for the thin products. Then, we can compute the convolution explicitly and regard the thin walls as cut from the domes with the same radii, and the same input function $f(\theta, \varphi)$ as in Eq. (11) can be applied.

For the transfer function $g(\theta, \varphi)$, Eq. (5) is used since the printing mechanism is the same and only the shapes and sizes change. Thus, the additive term $h_1(\theta, \varphi)$ is fully specified.

Next, we need to specify the sharp transition angles ϑ_j and n used in the 3D cookie-cutter function $h_2(\theta,\varphi)$ in Eq. (9). As shown in Fig. 2, n=4 and the angles are $\vartheta_1=\arctan(D/(2r_0\sin\varphi)),\ \vartheta_2=\pi-\vartheta_1,\ \vartheta_3=\pi+\vartheta_1,\ \vartheta_4=2\pi-\vartheta_1$ according to the geometry of the thin walls.

To capture the arch pattern of thin walls presented in the deformation profiles in Fig. 3, we choose $h_3(\theta, \varphi)$ as

$$h_{3}(\theta,\varphi) = \left\{ \sin\left(\frac{n}{4}\theta\right) \mathbf{1}_{\theta \in [\vartheta_{1},\vartheta_{2})} + \sin\left[\frac{n}{4}(\theta - \pi)\sin\varphi\right] \mathbf{1}_{\theta \in [\vartheta_{3},\vartheta_{4})} \right\} \sin\varphi,$$
(13)

where n is the number of sides. For the thin walls, we have n=4, and when $n\to\infty$, this term becomes white noise.

We follow similar assumptions as in [9] to incorporate the size effect, i.e.,: $\alpha_0(r_0) = a_1 + a_2r_0$; $\alpha_1(r_0) = b_1 + b_2r_0$; $n_1(r_0) = c_1 + c_2r_0$; n_2 and ψ are unknown constants; $\alpha_2(r_0) = d_1 + d_2r_0$; and $\alpha_3(r_0) = e_1 + e_2r_0$.

Note that the first four conjectures are for the spherical shape deformation model, and the last two would affect the deformation modeling for thin walls. Under these conjectures, at least two samples of each shape are required to estimate the model parameters.

 $\label{eq:table I} \textbf{TABLE I}$ Estimation for Dome Shape Deformation

| Estimate | Standard Error |
|----------|--|
| 0.6472 | 0.005970 |
| 4.0759 | 0.015579 |
| 0.0071 | 0.000204 |
| 0.0044 | 0.000161 |
| 0.0068 | 0.000598 |
| 0.0153 | 0.000488 |
| -0.0022 | 0.160061 |
| -0.0004 | 0.116186 |
| 0.0065 | 0.000046 |
| | 0.6472 4.0759 0.0071 0.0044 0.0068 0.0153 -0.0022 -0.0004 |

To obtain one unified model for all shapes considering the size effect, we apply a three-step physics-informed sequential model-fitting strategy as an extension to the method proposed in [9]. First, we fit the parametric model without Gaussian process for the deformation of domes because we treat the spherical shape as the base model. Second, we fix the parameters estimated in the previous step and fit the parameters of the thin wall shape while ignoring the Gaussian process. Third, we fit a GPR to the residuals of the parametric models for both shapes.

To avoid overfitting, we iteratively fit the parameters in g, i.e., (n_2, ψ, c_1, c_2) through maximum likelihood (MLE) and parameters for the coefficients, i.e., (a_1, a_2, b_1, b_2) through least square (LSE). The estimates for the spherical shape deformation model are given in Table I and the measured

shape deformations (in black) and model predictions (in blue) are superimposed in Fig. 4. The mean absolute error (MAE) is 0.0048 and the root mean square error (RMSE) is 0.0065. Note that the results are different from [9] since the input function $f(\theta,\varphi)$ is changed to Eq. (11). Also, we could ignore the term c_1 and c_2 and simplify function g as $g(\theta,\varphi)=1+\cos(n_2\theta+\psi)$ since their estimates are insignificant.

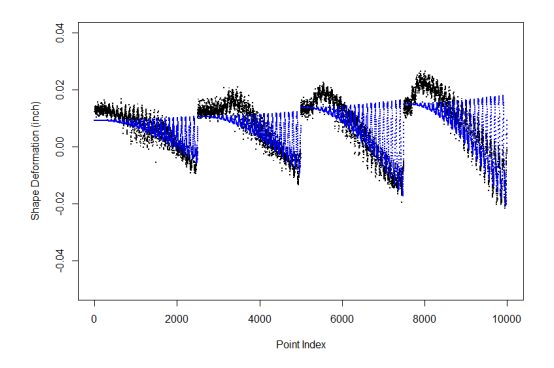


Fig. 4. Measured shape deformation (in black) and model prediction (in blue) for domes

The thin walls with radii of 0.8 inch and 2.0 inch are used as the training set, and the 1.5-inch thin wall is the validation set. The estimated model parameters for α_2 and α_3 are shown in Table II, and the measured deformations versus model predictions are presented in Fig. 5. For this model, the MAE is 0.0137 and the RMSE is 0.0192. The performance of the parametric part of the model is worse for the thin walls than for the spherical shapes.

TABLE II
MLE ESTIMATION FOR THIN WALL SHAPE DEFORMATION

| Parameters | Estimate | Standard Error |
|------------|----------|----------------|
| d_1 | -0.0614 | 0.001394 |
| d_2 | 0.0118 | 0.000857 |
| e_1 | 0.0459 | 0.002459 |
| e_2 | -0.0044 | 0.001542 |
| σ | 0.0113 | 0.000115 |

It is obvious that there are some remaining spatial patterns to be captured, so the residuals are fitted with GPR. The squared-exponential kernel is used with the form [29]

$$k(\mathbf{x_i}, \mathbf{x_j} | \sigma_f, \sigma_l) = \sigma_f^2 \exp\left(-\frac{1}{2} \frac{d(\mathbf{x_i}, \mathbf{x_j})}{\sigma_l^2}\right),$$
 (14)

where $d(\mathbf{x_i}, \mathbf{x_j})$ is the distance between two samples x_i and x_j . To more accurately describe the spatial correlation between two sample points, we first transform each point to the Cartesian coordinate system, i.e., $\mathbf{x_i} = (x_i, y_i, z_i)$. Then the coordinates are standardized and the Euclidean distances between points are computed.

The residuals for all four domes and three thin walls except the one with radius of 1.5 inches are used as the training set, and the 1.5-inch thin wall with a half-cylindrical shape is left as the validation set. The estimated parameters are $\sigma_f=0.0098$, $\sigma_l=0.2269$ and $\sigma=0.0085$, and the model has MAE = 0.0047 and RMSE = 0.0078. The measurements and model predictions are presented in Fig. 6 and Fig. 7. Since the Gaussian process combines the point coordinates information of all shapes together, and the points on the smaller domes are closer to those on the thin walls, 0.5-inch and 0.8-inch dome deformation predictions are greatly affected by the deformation pattern of thin walls.

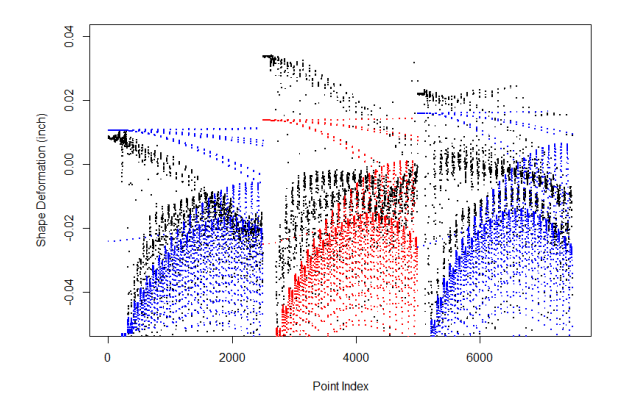


Fig. 5. Measured shape deformation (in black), training set prediction (in blue) and validation set prediction (in red) for thin walls

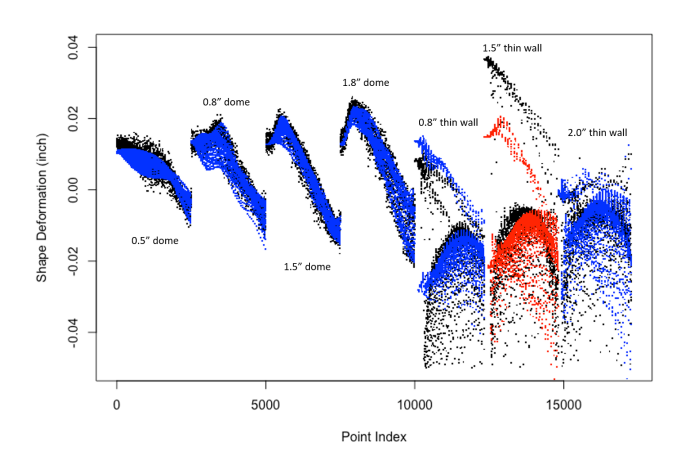


Fig. 6. Measured shape deformation (in black), training set prediction (in blue) and validation set prediction (in red) after adding GPR

IV. CONCLUSION

This work extends the convolution learning framework for shape deviation modeling by enabling joint learning for a wide class of 3D shapes including both spherical and polyhedral shapes. The newly developed 3D cookie-cutter function can effectively capture the unique pattern of the shape deformation for polyhedral shapes. The case study shows that the unified model can successfully predict the shape deformation of both domes and thin wall shapes. Since 3D freeform shapes can be approximated as a combination of spherical and polyhedral patches, the extended convolution learning framework builds a foundation for modeling and

predicting the quality of 3D freeform shapes. Lastly, the current Gaussian process regression methodology overestimates the correlations among different shapes, and it can be improved by changing the kernel function and considering new distance measures for points from different shapes.

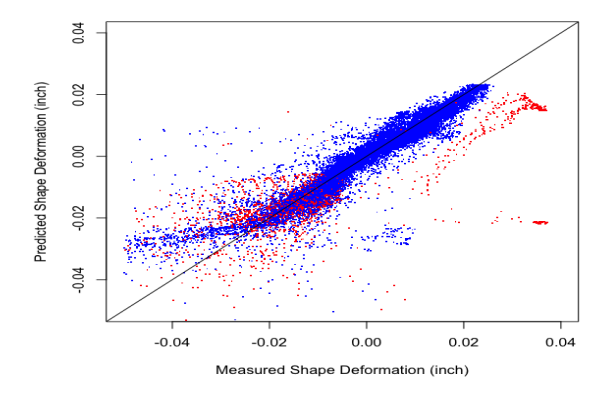


Fig. 7. Measured shape deformation vs. model prediction for all shapes (training set in blue and validation set in red)

ACKNOWLEDGMENT

This work is supported by US National Science Foundation with grant NSF CMMI-1901514. The experimental work was conducted in Prof. Yong Chen's lab at University of Southern California.

REFERENCES

- [1] B. P. Conner, G. P. Manogharan, A. N. Martof, L. M. Rodomsky, C. M. Rodomsky, D. C. Jordan, and J. W. Limperos, "Making sense of 3-d printing: Creating a map of additive manufacturing products and services," *Additive Manufacturing*, vol. 1-4, pp. 64–76, 2014.
- [2] W. Gao, Y. Zhang, D. Ramanujan, K. Ramani, Y. Chen, C. B. Williams, C. C. Wang, Y. C. Shin, S. Zhang, and P. D. Zavattieri, "The status, challenges, and future of additive manufacturing in engineering," *Computer-Aided Design*, vol. 69, pp. 65–89, 2015.
- [3] Q. Huang, J. Zhang, A. Sabbaghi, and T. Dasgupta, "Optimal offline compensation of shape shrinkage for three-dimensional printing processes," *IIE Transactions*, vol. 47, no. 5, pp. 431–441, 2015.
- [4] Q. Huang, H. Nouri, K. Xu, Y. Chen, S. Sosina, and T. Dasgupta, "Statistical predictive modeling and compensation of geometric deviations of three-dimensional printed products," *Journal of Manufacturing Science and Engineering, Transactions of the ASME*, vol. 136, no. 6, pp. 1–10, 2014.
- [5] H. Luan and Q. Huang, "Prescriptive modeling and compensation of in-plane shape deformation for 3-D printed freeform products," *IEEE Transactions on Automation Science and Engineering*, vol. 14, no. 1, pp. 73–82, 2017.
- [6] M. Khanzadeh, P. Rao, R. Jafari-Marandi, B. K. Smith, M. A. Tschopp, and L. Bian, "Quantifying geometric accuracy with unsupervised machine learning: Using self-organizing map on fused filament fabrication additive manufacturing parts," *Journal of Manufacturing Science and Engineering, Transactions of the ASME*, vol. 140, no. 3, 2017.
- [7] A. Sabbaghi and Q. Huang, "Model transfer across additive manufacturing processes via mean effect equivalence of lurking variables," Annals of Applied Statistics, vol. 12, no. 4, pp. 2409–2429, 2018.
- [8] B. M. Colosimo, Q. Huang, T. Dasgupta, and F. Tsung, "Opportunities and challenges of quality engineering for additive manufacturing," *Journal of Quality Technology*, vol. 50, no. 3, pp. 233–252, 2018.
- [9] Q. Huang, Y. Wang, M. Lyu, and W. Lin, "Shape Deviation Generator-A Convolution Framework for Learning and Predicting 3-D Printing Shape Accuracy," *IEEE Transactions on Automation Science and Engineering*, vol. 17, no. 3, pp. 1486–1500, 2020.

- [10] C. Liu, Z. J. Kong, S. Babu, C. Joslin, and J. Ferguson, "An integrated manifold learning approach for high-dimensional data feature extractions and its applications to online process monitoring of additive manufacturing," *IISE Transactions*, vol. 0, no. 0, pp. 1–21, 2021.
- [11] L.-E. Lindgren, A. Lundbäck, M. Fisk, R. Pederson, and J. Andersson, "Simulation of additive manufacturing using coupled constitutive and microstructure models," *Additive Manufacturing*, vol. 12, pp. 144–158, 2016.
- [12] J. C. Steuben, A. J. Birnbaum, J. G. Michopoulos, and A. P. Iliopoulos, "Enriched analytical solutions for additive manufacturing modeling and simulation," *Additive Manufacturing*, vol. 25, pp. 437–447, 2019.
- [13] W. E. King, A. T. Anderson, R. M. Ferencz, N. E. Hodge, C. Kamath, S. A. Khairallah, and A. M. Rubenchik, "Laser powder bed fusion additive manufacturing of metals; physics, computational, and materials challenges," *Applied Physics Reviews*, vol. 2, no. 4, p. 041304, 2015.
- [14] W. Yan, S. Lin, O. L. Kafka, Y. Lian, C. Yu, Z. Liu, J. Yan, S. Wolff, H. Wu, E. Ndip-Agbor, M. Mozaffar, K. Ehmann, J. Cao, G. J. Wagner, and W. K. Liu, "Data-driven multi-scale multi-physics models to derive process–structure–property relationships for additive manufacturing," *Computational Mechanics*, vol. 61, no. 5, pp. 521–541, 2018.
- [15] S. K. Everton, M. Hirsch, P. Stravroulakis, R. K. Leach, and A. T. Clare, "Review of in-situ process monitoring and in-situ metrology for metal additive manufacturing," *Materials & Design*, vol. 95, pp. 431–445, 2016.
- [16] D. A. Anderegg, H. A. Bryant, D. C. Ruffin, S. M. Skrip, J. J. Fallon, E. L. Gilmer, and M. J. Bortner, "In-situ monitoring of polymer flow temperature and pressure in extrusion based additive manufacturing," *Additive Manufacturing*, vol. 26, pp. 76–83, 2019.
- [17] H. Mao, T.-H. Kwok, Y. Chen, and C. C. Wang, "Adaptive slicing based on efficient profile analysis," *Computer-Aided Design*, vol. 107, pp. 89–101, 2019.
- [18] J. Francis and L. Bian, "Deep Learning for Distortion Prediction in Laser-Based Additive Manufacturing using Big Data," *Manufacturing Letters*, vol. 20, pp. 10–14, 2019.
- [19] N. Decker, M. Lyu, Y. Wang, and Q. Huang, "Geometric Accuracy Prediction and Improvement for Additive Manufacturing Using Triangular Mesh Shape Data," *Journal of Manufacturing Science and Engineering*, vol. 143, no. 6, pp. 1–12, 2021.
- [20] L. Cheng, K. Wang, and F. Tsung, "A hybrid transfer learning framework for in-plane freeform shape accuracy control in additive manufacturing," *IISE Transactions*, vol. 53, no. 3, pp. 298–312, 2020.
- [21] R. D. S. B. Ferreira, A. Sabbaghi, and Q. Huang, "Automated Geometric Shape Deviation Modeling for Additive Manufacturing Systems via Bayesian Neural Networks," *IEEE Transactions on Automation Science and Engineering*, vol. 17, no. 2, pp. 584–598, 2020.
- [22] Q. Huang, "An Analytical Foundation for Optimal Compensation of Three-Dimensional Shape Deformation in Additive Manufacturing," *Journal of Manufacturing Science and Engineering, Transactions of the ASME*, vol. 138, no. 6, pp. 1–8, 2016.
- [23] Y. Jin, S. J. Qin, and Q. Huang, "Out-of-plane geometric error prediction for additive manufacturing," in 2015 IEEE International Conference on Automation Science and Engineering (CASE), 2015, pp. 918–923.
- [24] ——, "Prescriptive analytics for understanding of out-of-plane deformation in additive manufacturing," in 2016 IEEE International Conference on Automation Science and Engineering (CASE), 2016, pp. 786–791.
- [25] Y. Jin, S. Joe Qin, and Q. Huang, "Offline predictive control of outof-plane shape deformation for additive manufacturing," *Journal of Manufacturing Science and Engineering, Transactions of the ASME*, vol. 138, no. 12, 2016.
- [26] Y. Jin, S. J. Qin, and Q. Huang, "Modeling inter-layer interactions for out-of-plane shape deviation reduction in additive manufacturing," *IISE Transactions*, vol. 52, no. 7, pp. 721–731, 2020.
- [27] T. Hastie, R. Tibshirani, and J. Friedman, The elements of statistical learning: data mining, inference, and prediction. Springer Science & Business Media, 2009.
- [28] P. J. Besl and N. D. McKay, "Method for registration of 3-D shapes," in *Sensor Fusion IV: Control Paradigms and Data Structures*, P. S. Schenker, Ed., vol. 1611, International Society for Optics and Photonics. SPIE, 1992, pp. 586 – 606.
- [29] C. E. Rasmussen and C. K. I. Williams, Gaussian Processes for Machine Learning. MIT Press, 2006.